

# Inactivation of *Rai1* in mice recapitulates phenotypes observed in chromosome engineered mouse models for Smith–Magenis syndrome

Weimin Bi<sup>1</sup>, Tomoko Ohyama<sup>1</sup>, Hisashi Nakamura<sup>1</sup>, Jiong Yan<sup>1</sup>, Jaya Visvanathan<sup>1</sup>,  
Monica J. Justice<sup>1</sup> and James R. Lupski<sup>1,2,3,\*</sup>

<sup>1</sup>Department of Molecular and Human Genetics, <sup>2</sup>Department of Pediatrics, Baylor College of Medicine and  
<sup>3</sup>Texas Children's Hospital, Houston, TX 77030, USA

Received December 10, 2004; Revised February 14, 2005; Accepted February 22, 2005

Retinoic acid induced 1 (*RAI1*) is among the 20 genes identified in the critical region of Smith–Magenis syndrome (SMS), a genomic disorder with multiple congenital anomalies associated with a 3.7 Mb heterozygous deletion of 17p11.2. Heterozygous premature termination mutations in *RAI1* have been identified recently in SMS patients without detectable deletions. To investigate *Rai1* function, we generated a null allele in mice by gene targeting and simultaneously inserted a *lacZ* reporter gene into the *Rai1* locus. X-gal staining of the *Rai1*<sup>+/-</sup> mice recapitulated the endogenous expression pattern of *Rai1*. The gene was predominantly expressed in the epithelial cells involved in organogenesis. Obesity and craniofacial abnormalities, which have been reported in SMS mouse models containing a heterozygous deletion of the syntenic SMS critical region, were observed in *Rai1*<sup>+/-</sup> mice. Thus, haploinsufficiency of *Rai1* causes obesity and craniofacial abnormalities in mice. Interestingly, the penetrance of craniofacial anomalies is further reduced in *Rai1*<sup>+/-</sup> mice. Most homozygous mice died during gastrulation and organogenesis. The surviving *Rai1*<sup>-/-</sup> mice were growth retarded and displayed malformations in both the craniofacial and the axial skeleton. Using green fluorescence protein and GAL4 DNA binding domain fusions to *Rai1*, we showed that *Rai1* is translocated to the nucleus and it has transactivation activity. Our data are consistent with *Rai1* functioning as a transcriptional regulator, document that *Rai1* haploinsufficiency is responsible for obesity and craniofacial phenotypes in mice with SMS deletions, and indicate *Rai1* is important for embryonic and postnatal developments.

## INTRODUCTION

Smith–Magenis syndrome (SMS, MIM 182290) is characterized by multiple congenital anomalies and mild-mental retardation. The common clinical characteristics (>75%) include distinct craniofacial and skeletal anomalies, neurobehavioral features such as self-injurious behavior and sleep disturbance (1,2). An interstitial deletion of a 3.7 Mb genomic fragment in one allele of chromosome 17 band p11.2 was identified in most patients.

This common deletion derives from non-allelic homologous recombination between the flanking low-copy repeats termed proximal and distal SMS-REPs (3–7). The predicted reciprocal duplication leads to the dup(17)(p11.2p11.2) syndrome with a

less severe phenotype than SMS (8). By analyzing the patients with unusual sized deletions, the smallest region of overlap or SMS critical region (SMCR) was confined to an ~1.1 Mb region that contains 20 genes (9) and independently to an ~950 kb interval (10). Frameshift and nonsense mutations in *RAI1*, a gene that lies in the SMCR, were identified in five SMS patients (11,12), suggesting that *RAI1* haploinsufficiency is responsible for the predominant neurobehavioral, craniofacial and otolaryngological features of the syndrome.

Human 17p11.2 is highly conserved and syntenic to the mouse chromosome 11, 32–34 centimorgan region, making it feasible to establish a mouse model for SMS (9). Using chromosome engineering, *Df(11)17* mice, containing an ~2 Mb deletion of the syntenic region of the human SMS

\*To whom correspondence should be addressed at: Department of Molecular and Human Genetics, Baylor College of Medicine, Room 604B, One Baylor Plaza, Houston, TX 77030-3498, USA. Tel: +1 7137986530; Fax: +1 7137985073; Email: jlupski@bcm.tmc.edu

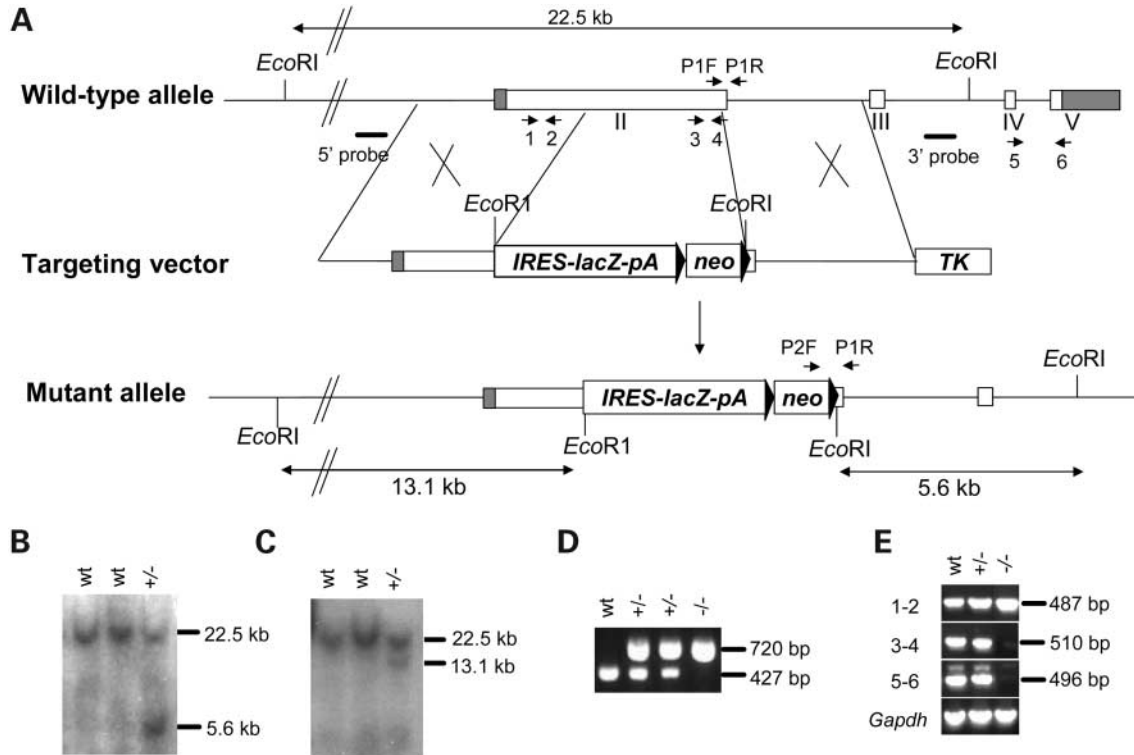


**Figure 1.** Generation of *Rail* mutant mice. (A) Strategy to mutate *Rail* by gene targeting. An ~4.0 kb portion of the coding region in exon 2 was replaced by an internal ribosome entry site *IRES-lacZ-pA* cassette followed by a loxP flanked *PGKneobpA* cassette. An *MC1tkpA* cassette was added next to the 3'-arm of homology. (B and C) The *Rail* mutant allele was identified by Southern blot analysis. Genomic DNA from targeted ES cells was digested with *EcoRI*. A 5.6 kb band was observed for the targeted allele when hybridized using the 3'-probe (B) and a 13.1 kb band when using 5'-probe (C). (D) *Rail*<sup>+/-</sup> mice were identified by PCR using primers P1F and P1R for the amplification of a 427 bp fragment from the wild-type allele and primers P2F and P1R for a 720 bp fragment from the mutant allele. (E) RT-PCR on total RNA prepared from the kidneys.

common deletion, have been generated (13). The *Df(11)17/+* mice partially recapitulate the SMS phenotype with craniofacial abnormalities, obesity, seizures and neurobehavioral abnormalities including an abnormal circadian rhythm (13,14). Smaller deletions in mice were generated using retrovirus mediated chromosome engineering (15). Obesity and craniofacial abnormalities have also been observed in these animals, suggesting that the genes responsible for the craniofacial features and obesity are located in the small deletions (15). The craniofacial phenotype was strongly affected by genetic background and the size of the deletions (15). The role of segmental aneuploidy versus single gene haploinsufficiency in expression and penetrance of the full phenotype remains unclear for both humans and mice.

Little is known about the cellular and developmental role of RAI1. Expression of *GT1*, a splice variant of *Rail* (12,16) was markedly up-regulated by treatment with retinoic acid in a mouse carcinoma cell line P19 (16). A polymorphic CAG-repeat is present in the N-terminus of the RAI1 protein, the length of which is associated with the age at onset of spinocerebellar ataxia type 2 (17) and the response to neuroleptic medication in schizophrenia (18). Bioinformatic analyses suggest that RAI1 might be a transcriptional regulator (11,12). RAI1 contains several patches of >50% similarity with TCF20, a transcriptional cofactor, and these two genes have a similar gene structure. RAI1 has two putative bipartite nuclear localization signals (NLSs). Furthermore, in the C-terminus of both human

and mouse RAI1, we identified a zinc finger like plant homeo domain (PHD), which is also present in the trithorax family of chromatin remodeling transcriptional regulators (12).

To elucidate the function of *RAI1* and the etiology of SMS, we generated a potential null *Rail* allele by gene targeting. The heterozygous mice exhibited obesity and craniofacial phenotypes, and the homozygous mice displayed embryonic lethality and postnatal growth retardation. We also performed functional mapping studies using *Rail*-green fluorescence protein (GFP) fusion constructs and show that *Rail* is located in the nucleus with four NLSs. Moreover, we show that *Rail* has moderate but consistent transactivation activity in its N-terminus in a luciferase reporter assay. Our results demonstrate that *Rail* haploinsufficiency causes craniofacial phenotypes and obesity in both humans and mice, further support a role for RAI1 as a transcriptional regulator, and indicate that *Rail* is indispensable for embryonic development.

## RESULTS

### Targeted disruption of *Rail* in mice

To study the function of *Rail* *in vivo*, we inactivated it in mice. We inserted the *Escherichia coli lacZ* coding sequence and a *neo<sup>R</sup>* expression cassette into *Rail* exon 2 and simultaneously deleted 3910 bp nucleotides of *Rail* encoding residues 537–1790 (Fig. 1A). Recombination events at the

*Rail* locus were identified by Southern blot analysis of *Eco*R1-digested genomic DNA. The expected 5.6 kb fragment when hybridized with a 625 bp probe in intron 3 and 13.1 kb fragment with a 699 bp probe from intron 1 corresponding to the mutant allele, as well as the 22.5 kb fragment corresponding to the wild-type allele, were observed in the DNA from targeted cells (Fig. 1B and C). Twelve percent of the ES cell clones showed the expected results for the homologous recombination event. As shown by RT-PCR (Fig. 1D), only the 5'-undeleted region was retained in the transcript from the targeted allele. This predicted truncation eliminates all the nuclear localization regions and the PHD domain, which suggests that the targeted allele is a null allele.

Three independent targeted clones were injected into C57BL/6 blastocysts and all led to germline transmission. Mice were genotyped by PCR amplification of genomic DNA using primers P1F and P1R for a 720 bp fragment corresponding to the mutant allele and a 427 bp fragment corresponding to the wild-type allele (Fig. 1D). Heterozygous mice are viable and fertile.

### Expression of *Rail* during embryogenesis

The inserted *lacZ* reporter gene is under the control of the *Rail* promoter. We examined the expression of the *lacZ* reporter gene in *Rail*<sup>+/-</sup> embryos by X-gal staining (Fig. 2). At 10.5 dpc, the blue staining was predominantly observed in the craniofacial components derived from branchial arches and limb buds (Fig. 2A). A similar expression pattern was observed for *Rail* by whole-mount *in situ* hybridization using a probe specific to the *Rail* or *Gtl* (Fig. 2B), confirming that the X-gal staining pattern in *Rail*<sup>+/-</sup> embryos recapitulated the expression pattern of *Rail*. X-gal staining showed that *Rail* was expressed mainly in the branchial arches and otic vesicles at 9.5 dpc (Fig. 2C). Broader expression was observed in 12.5 dpc embryos. However, the expression level was not evenly distributed among tissues. For example, the expression level in the mesenchymal condensation in the limb buds was much stronger than that in the surrounding tissues (Fig. 2D). Sections of X-gal stained embryos showed that in 10.5 dpc embryos *Rail* was predominantly expressed in epithelial cells such as the epithelium lining the olfactory pit and nasal process, endoderm of branchial arches, the apical ectodermal ridge (AER), gut, Rathke's pouch and the thyroid primordium (Fig. 2E-G).

### Obesity in *Rail*<sup>+/-</sup> mice

SMS patients are often overweight. Obesity has been reported in SMS mouse models including *Df(11)17/+* mice (13) and mice with the smaller deletions (15). *Rail* lies within the genetic interval deleted in these hemizygous animal models. We measured the body weight of *Rail*<sup>+/-</sup> mice and their littermates from ages 3 weeks to 7 months (Fig. 3). Significant weight differences began to be observed at 20 weeks of age in the heterozygous males and 23 weeks in females. Both sexes of *Rail*<sup>+/-</sup> animals were overweight compared with littermate controls although the heterozygous mice were noticeably underweight at 4-7 weeks of age. The distribution of the body weight of the heterozygous mice was much broader than that of the wild-type after 10 weeks of age,

which is reflected in the larger standard error (Fig. 3). These results indicate that *Rail* contributes to obesity reported in the mouse models with deletions. This suggests that haploinsufficiency of *RAI1* is a major cause for the obesity observed in many SMS patients.

### Craniofacial anomalies in *Rail*<sup>+/-</sup> mice

SMS patients display distinct craniofacial features including midface hypoplasia, a broad nasal bridge, brachycephaly, prognathia and abnormal external ears (1,2,4,19). The majority (70-80%) of *Df(11)17/+* mice consisting of a strain background of 75% C57BL6/25% 129SvEv at the N2 generation exhibited craniofacial phenotypes (Table 1) such as hypertelorism (broader distance between the eyes) and shorter and broader snouts (13). Similar phenotypes were observed in mice with the smaller deletions but with reduced penetrance (33%) and severity (15). We evaluated the faces of 56 *Rail*<sup>+/-</sup> mice at 4 months of age by visual inspection at the N2 generation. Ten (18%) heterozygous mice showed obvious shorter and broader snouts than their wild-type littermates (Table 1). Fewer *Rail*<sup>+/-</sup> mice (7%) exhibited craniofacial defects in the F2 generation (Table 1). In these mice with craniofacial defects, the snouts were short and sometimes concave (Fig. 4). In addition, the snouts were curved to the left or right. We observed such craniofacial features in only one mouse out of more than 60 wild-type littermates in the N2 generation. The craniofacial anomalies were discernable as early as 21 days of age at the time of weaning.

Skeletal analysis indicated that the craniofacial defects were mainly caused by the malformation of the craniofacial skeletal elements. Three landmarks were selected to measure the length of the nasal bones (distances between a to b and c to b) and the distance between the eyes (distances from a to c) (Fig. 4), which have been shown to be significantly different between the mice with smaller deletions and wild-type littermates (15). The nasal bones in the *Rail*<sup>+/-</sup> mice with craniofacial abnormalities were shorter and broader than those observed in the wild-type (Fig. 4). The craniofacial evaluation based on visual inspection was quite consistent with that determined by skeletal measurements. The mice with shorter snouts at weaning also exhibited shorter nasal bones.

### Embryonic lethality and postnatal growth retardation in *Rail*<sup>-/-</sup> mutants

Genotype analysis of 400 individual mice representing the F1 of heterozygous parents revealed frequencies significantly different from those expected by Mendelian segregation of the mutant allele (+/+ 36.2%, +/- 59.3%, -/- 4.5%), indicating that the lack of *Rail* results in embryonic lethality for the vast majority of *Rail* homozygous mutants.

To determine when the *Rail*<sup>-/-</sup> mice die during embryonic development, we performed timed matings of heterozygous mice (Table 2). Between 15.5 and 18.5 dpc, only two (3.3% relative to live embryos genotyped) homozygous mutant embryos were recovered from 59 live embryos examined. Eleven embryos were almost completely resorbed. The frequency of homozygous mutants was similar to that of live born mice, suggesting most homozygous mutants died

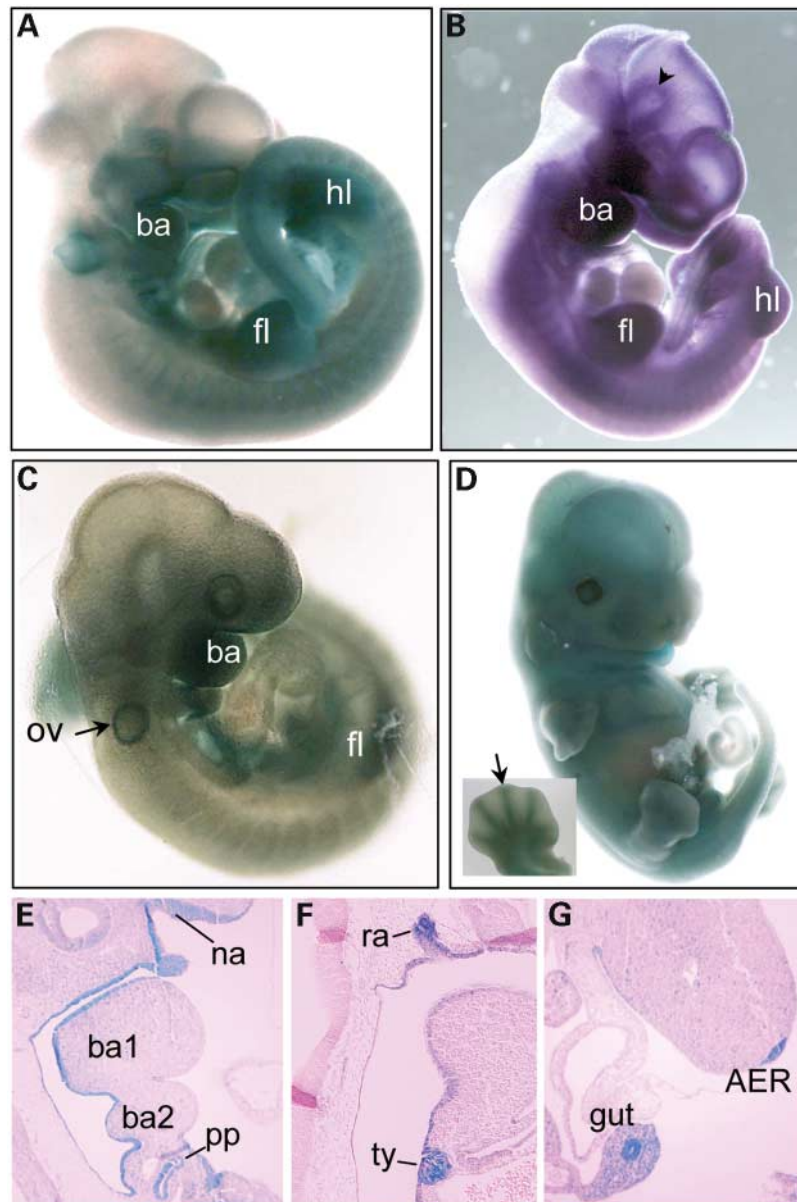


**Figure 2.** Embryonic expression of *Rai1* visualized by X-gal staining. (A, C and D) X-gal staining of *Rai1*<sup>+/-</sup> embryos at 10.5 dpc (A), 9.5 dpc (C) and 12.5 dpc (D). At 10.5 dpc, blue staining was predominantly observed in craniofacial components derived from branchial arches (br), forelimb bud (fl) and hindlimb bud (hl). The pattern of X-gal staining recapitulates the *Rai1* mRNA expression in 10.5 dpc embryos (B) showed by whole-mount *in situ* hybridization. Note that the staining in the midbrain (arrowhead in B) is non-specific. The insert in (D) indicates the blue staining in mesenchymal condensations (arrow) in the developing limb. (E–G) Sections of the X-gal stained *Rai1*<sup>+/-</sup> embryo at 10.5 dpc showed that *Rai1* was expressed in the epithelium lining olfactory pit and nasal process (na), endoderm of branchial arches, Rathke's pouch (ra), the thyroid primordium (ty), AER and gut. ov, otic vesicle; pp, pharyngeal pouches; ba1, the first branchial arch; ba2, the second branchial arch.

before 15.5 dpc. Further genotyping of embryos at earlier stages showed that the amount of homozygous mutants gradually increased from 4.5% at 11.5 dpc to 14.2% at 8.5 dpc. There were many embryos resorbed even at 8.5 dpc. At 7.5 dpc, 11 (16.1%) embryos were homozygous mutants and no embryos were detectable in five deciduum. The total number of homozygous mutants, including the presumably resorbed ones, was 16 (23.5%) similar to that expected by Mendelian segregation and suggesting that implantation is not affected in the homozygous mutants. Thus, a significant

number of the homozygous embryos died during gastrulation and organogenesis, after implantation.

Of 13 *Rai1*<sup>-/-</sup> mice that survived beyond birth, six of them died shortly after birth or within a few days after birth, with another six dying around the age of weaning. Only one survived after 3 months. At the end of their lifespan, they appeared weak and debilitated and manifested apparent severe dehydration and weight loss. The *Rai1*<sup>-/-</sup> mice did not have gross morphological abnormalities at birth, but exhibited growth retardation (Fig. 5A and B). The heterozygous

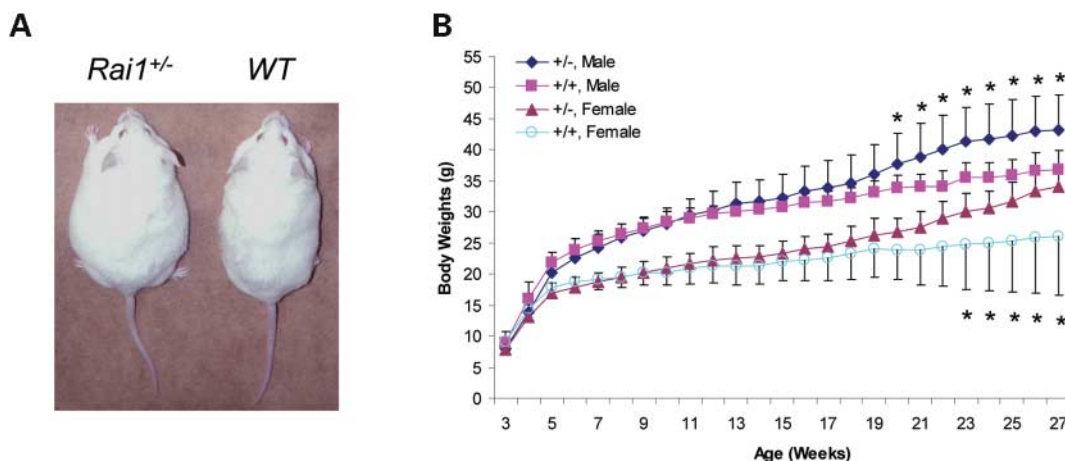


**Figure 3.** *Rai1*<sup>+/-</sup> mice are overweight in comparison to their wild-type littermates. (A) Photograph showing the body size of *Rai1*<sup>+/-</sup> and wild-type mice at 8 months of age. (B) Body weights of *Rai1*<sup>+/-</sup> and wild-type mice over the course of 27 weeks. The asterisk (\*) indicates the measurement at which the heterozygous mutants were significantly ( $P < 0.05$ ) heavier than the wild-type littermates. For males, wild-type,  $n = 15$ , *Rai1*<sup>+/-</sup>,  $n = 17$ ; for females, wild-type,  $n = 10$ , *Rai1*<sup>+/-</sup>,  $n = 11$ .

**Table 1.** Comparison of the penetrance of craniofacial abnormalities

Background	Generation	Strain	No. of mice evaluated	No. of mice with craniofacial phenotype	%
50% 129/ 50% C57	F2	<i>Rai1</i> <sup>+/-</sup>	29	2	7
	F1	<i>Df(11) - 1, 2/+</i>	70	7	10
	F1	<i>Df(11)17/+</i>	>50		>90
25% 129/ 75% C57	N2	<i>Rai1</i> <sup>+/-</sup>	56	10	18
	N2	<i>Df(11) - 1, 2/+</i>	54	18	33
	N2	<i>Df(11)17/+</i>	>50		70–80

The craniofacial phenotypes include the shorter and concaved nasal bones in *Rai1*<sup>+/-</sup> mice as illustrated in Figure 2F, with increased penetrance, for heterozygous deficiency mice containing a chromosome engineered deletion of the *Rai1* genomic region. Data for *Df(11)17/+*, *Df(11) - 1,2/+* are from (13,15).

mice weighed slightly less than their wild-type littermates from birth to 2 weeks of age. At birth, the *Rai1*<sup>+/-</sup> mice weighed ~78% of that of the wild-type littermates ( $P = 0.005$ ). By 2 weeks of age, their body weight was remarkably lower, only 41% of that of wild-type littermates. In addition, the *Rai1*<sup>+/-</sup> mice exhibited shorter snouts similar to what we observed in some *Rai1*<sup>+/-</sup> mice (Fig. 5C). Extra cartilaginous elements were observed in the digit 5 of both forelimbs in almost all *Rai1*<sup>+/-</sup> mutants at birth (Fig. 5D–F). We rarely observed this extra nubbin in *Rai1*<sup>+/-</sup> mutants (<5%), but never in their wild-type littermates.

#### Skeletal defects in *Rai1*<sup>+/-</sup> mice

We examined the skeletons of seven *Rai1*<sup>+/-</sup> mice at 20 days to 1.5 months of age for morphological changes. Craniofacial

abnormalities were observed in all of the surviving *Rai1*<sup>+/-</sup> mutants, and the defects look more severe than those observed in *Rai1*<sup>+/-</sup> mice. The nasal bone was much broader and shorter than that in their littermates (Fig. 6A–D). Four mice displayed curved nasal bones and misalignment of the upper and lower incisors (Fig. 6A, B, E and F). Lateral bending of the snouts was also observed in the *Rai1*<sup>+/-</sup> mice without misalignment, suggesting that it is the primary defect. The misalignment of incisors is likely due to the more pronounced bending of the snouts in the *Rai1*<sup>+/-</sup> mice.

In addition to craniofacial defects, the homozygous mutants exhibited defects in other skeletal components (Table 3). The thyroid bones in all the seven *Rai1*<sup>+/-</sup> mice were hypoplastic with the central bone parts of the thyroid bones not formed (Fig. 6G and H). The abnormalities of the thyroid bones are likely caused by *Rai1* deficiency in the pharyngeal pouches in which *Rai1* is prominently expressed. The 13th ribs were thinner and sometimes did not articulate with vertebral body (Fig. 6I and J). Although we did not observe any pattern changes, the homozygous mutants showed obvious malformations in axial skeleton (Fig. 6K–M). The odontoid process of the axis (C2) was fused with the facet of the atlas (C1), which limited the rotational movement of the head. The dorsal arches were frequently not closed in some cervical and thoracic vertebrae, and the spinal process was missing in the thoracic vertebra T2 (Fig. 6M). Examination of individual vertebra showed that in C4, C5 and C6 the transverse foramina, which form a canal that permits passage of the vertebral arteries and veins, were not closed (Fig. 6M). Thus, the skeletal anomalies in the *Rai1*<sup>+/-</sup> mice include the craniofacial defects that were also observed in the *Rai1*<sup>+/-</sup> mice and defects in axial skeleton that were not observed in the *Rai1*<sup>+/-</sup> mice.

#### *Rai1* is a nuclear protein with four NLS

Bioinformatic analyses suggest that RAI1 is involved in transcriptional regulation; it contains two bipartite nuclear localization sequences (11) and a single PHD domain (12).

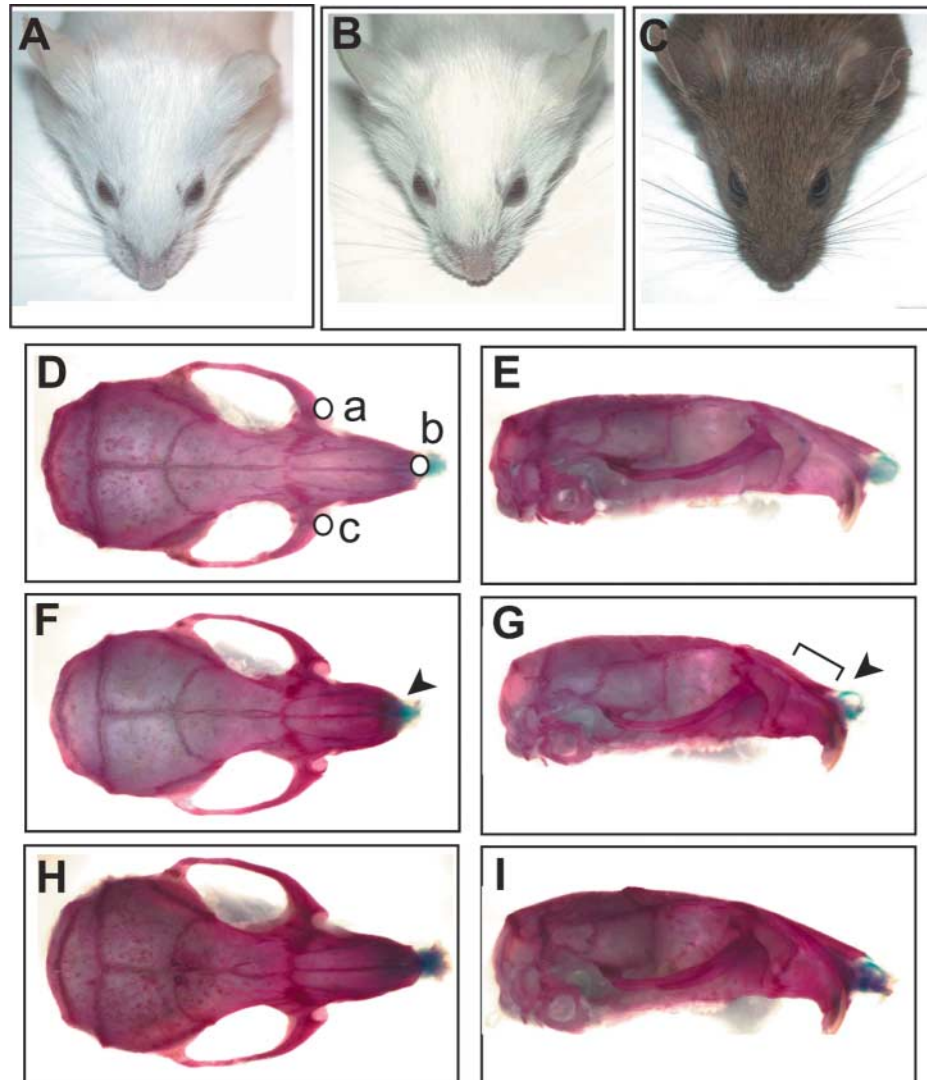


**Figure 4.** Craniofacial abnormalities in *Rai1*<sup>+/-</sup> mice. The snouts in a portion of heterozygous mice (**B**) were obviously concave and shorter than their wild-type littermates (**A**), whereas the other heterozygous mice exhibited quite normal snouts (**C**). Top views (**D**, **F**, **H**) and side views (**E**, **G**, **I**) of the skulls of wild-type (**D** and **E**), heterozygous mice with craniofacial phenotypes (**F**, **G**) and heterozygous mice without craniofacial abnormalities (**H** and **I**). Landmarks (circles) were selected to measure the length of the nasal bones (distances between a to b and c to b) and the distance between the eyes (distances from a to c). a and c, anterior notch on frontal process situated laterally in relation to the infraorbital fissure; b, nasale. The abnormal snouts were due to the shorter (arrowheads in **F**–**G**) and concaved (bracket in **G**) nasal bones in these heterozygous mice. The observation by visual inspection was consistent with the observation based on skeletal preparation.

**Table 2.** Genotype of offspring from heterozygous matings

Age	Number of pups				Total
	Wild-type	<i>Rai1</i> <sup>+/-</sup>	<i>Rai1</i> <sup>-/-</sup>	Resorbed	
NB	34	55	3 (3.3%)		92
15.5–18.5 dpc	13	44	2 (2.8%)	11	70
11.5 dpc	14	54	4 (4.5%)	16	88
10.5 dpc	9	36	4 (7.1%)	7	56
9.5 dpc	13	41	6 (8.8%)	8	68
8.5 dpc	28	52	15 (14.2%)	11	106
7.5 dpc	16	36	11 (16.1%)	5	68

The numbers in parentheses are percentage of the *Rai1*<sup>-/-</sup> mice over the total pups including the resorbed ones. dpc, days post-coitum; NB, 0–16 h after birth.

To determine the subcellular localization of Rai1, green fluorescence protein (GFP) was fused to the full-length Rai1 and the expression vector GFP-Rai1-(1–1890) was transiently transfected into HeLa cells (Fig. 7). Examination of GFP signal indicated that Rai1 is localized exclusively to the nucleus of HeLa cells. We also examined the localization of GT1, a C-terminal splice variant of Rai1 (Fig. 7). Full-length GT1–GFP fusion protein was also located to the nucleus exclusively. Thus, Rai1 is likely a nuclear protein.

The peptide sequences that determine the nuclear localization were mapped by fusion of different coding regions of Rai1 with GFP (Fig. 7). Two regions, residues 1134–1164 and 1203–1229, directed the fusion proteins exclusively to the nucleus. Each region contains a bipartite NLS predicted by computer analyses. Moreover, we found that two

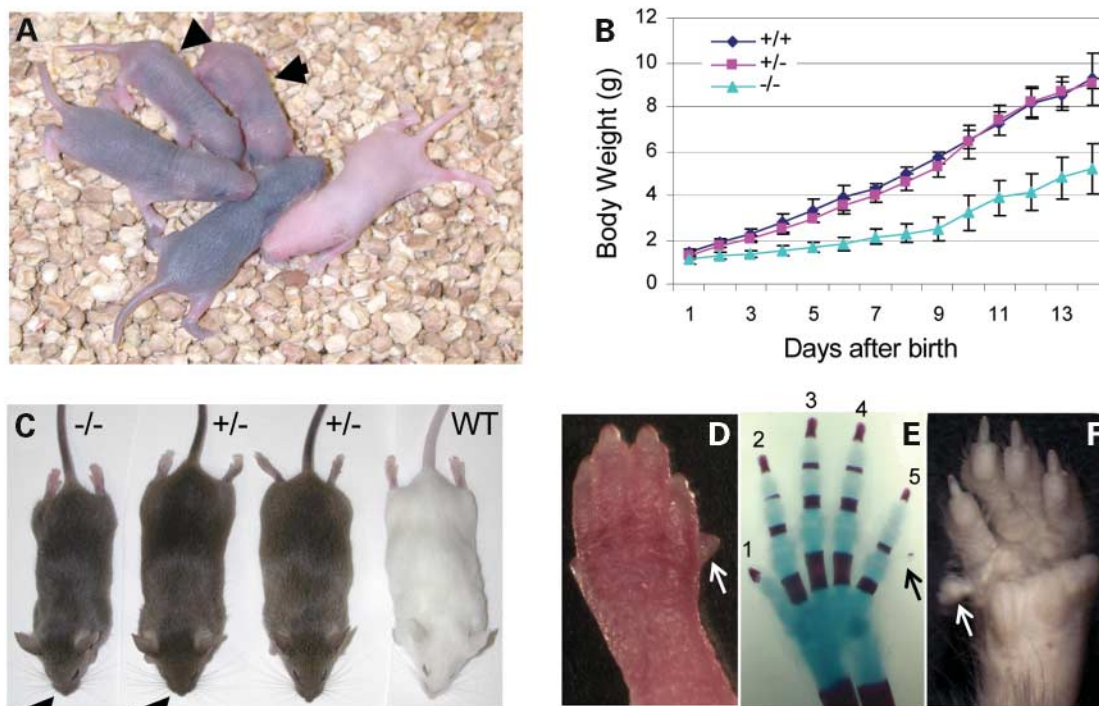


**Figure 5.** (A and B) The surviving *Rai1*<sup>-/-</sup> mice exhibited profound postnatal growth retardation. (A) Six-day-old mice. *Rai1*<sup>-/-</sup> mice (arrows) were smaller than their littermates. (B) Growth curve of the *Rai1*<sup>-/-</sup> ( $n = 6$ ), *Rai1*<sup>+/-</sup> ( $n = 9$ ) and wild-type ( $n = 8$ ) mice. *Rai1*<sup>-/-</sup> mice were significantly smaller than their wild-type littermates at birth. (C) Shorter snouts (arrowheads) were observed in a *Rai1*<sup>-/-</sup> and a *Rai1*<sup>+/-</sup> mouse in a litter of mice at 1 month of age but not in other *Rai1*<sup>+/-</sup> and wild-type littermates. (D–F) Extra nubbins (arrows) were observed in the digit 5 of the forelimbs in *Rai1*<sup>-/-</sup> mice at one day of age (D and E) and at 2 months of age (F), which were cartilaginous elements (E).

additional regions, 1246–1537 and 1537–1703, localized the GFP marker to the nucleus, indicating that there were four NLSs in total within *Rai1*. Peptides containing the regions unique to *Rai1* or GT1, residues 1703–1890 of *Rai1* and residues 1703–1841 of GT1, were localized to the cytoplasm.

### Two different transactivation domains are located in the N-terminus of *Rai1*

We hypothesized that *Rai1* is a transcriptional regulator (12). To examine whether *Rai1* has transactivation activity, full-length *Rai1* was fused with the GAL4 DNA binding domain (GAL4-BD) and co-transfected into HeLa cells with a luciferase reporter plasmid containing five tandem repeats of yeast GAL4-binding sites upstream of a promoter that controls the expression of the luciferase gene (Fig. 8). Reporter assays indicated that the full-length *Rai1* had transactivation activity with ~14-fold induction of transcription when 0.3  $\mu$ g of DNA was transfected (Fig. 8B). The putative transactivation domains in *Rai1* were mapped by fusion of different regions to GAL4-BD. The region containing residues 1–582, where the polymorphic poly-glutamine stretch is located, gave ~8-fold induction (Fig. 8C). A different region, residues 583–1142, gave ~20-fold induction. No transactivation was observed for the remaining region from amino acid 1126–1890. We conclude that *Rai1* is able to stimulate

transcriptional transactivation through its two N-terminal transactivation domains.

### DISCUSSION

Craniofacial anomalies and obesity are the features in SMS that were recapitulated in mice harboring hemizygous deletions syntenic to the human SMCR. We showed that *Rai1* haploinsufficiency in mice was associated with disease relevant craniofacial defects and obesity. Interestingly, the penetrance of the craniofacial phenotype was further reduced in *Rai1*<sup>+/-</sup> mice. The few homozygous mutant mice that survived exhibited growth retardation and defects in both the craniofacial and axial skeleton. Our data suggest that biallelic expression of *Rai1* or normal dosage of functional *Rai1* is required for the craniofacial development and body weight control.

### *Rai1* is the major gene responsible for the craniofacial defects and obesity

The craniofacial defects reported in the SMS mouse models with heterozygous deletions (13,15) were observed in a fraction of the *Rai1*<sup>+/-</sup> mice, suggesting that haploinsufficiency of *Rai1* causes the craniofacial phenotypes. These data support the findings in humans that the point mutations in *Rai1* led to the craniofacial phenotype and obesity in SMS (11,12).

Obesity represents a common health problem that is affected by both genetic and environmental factors.

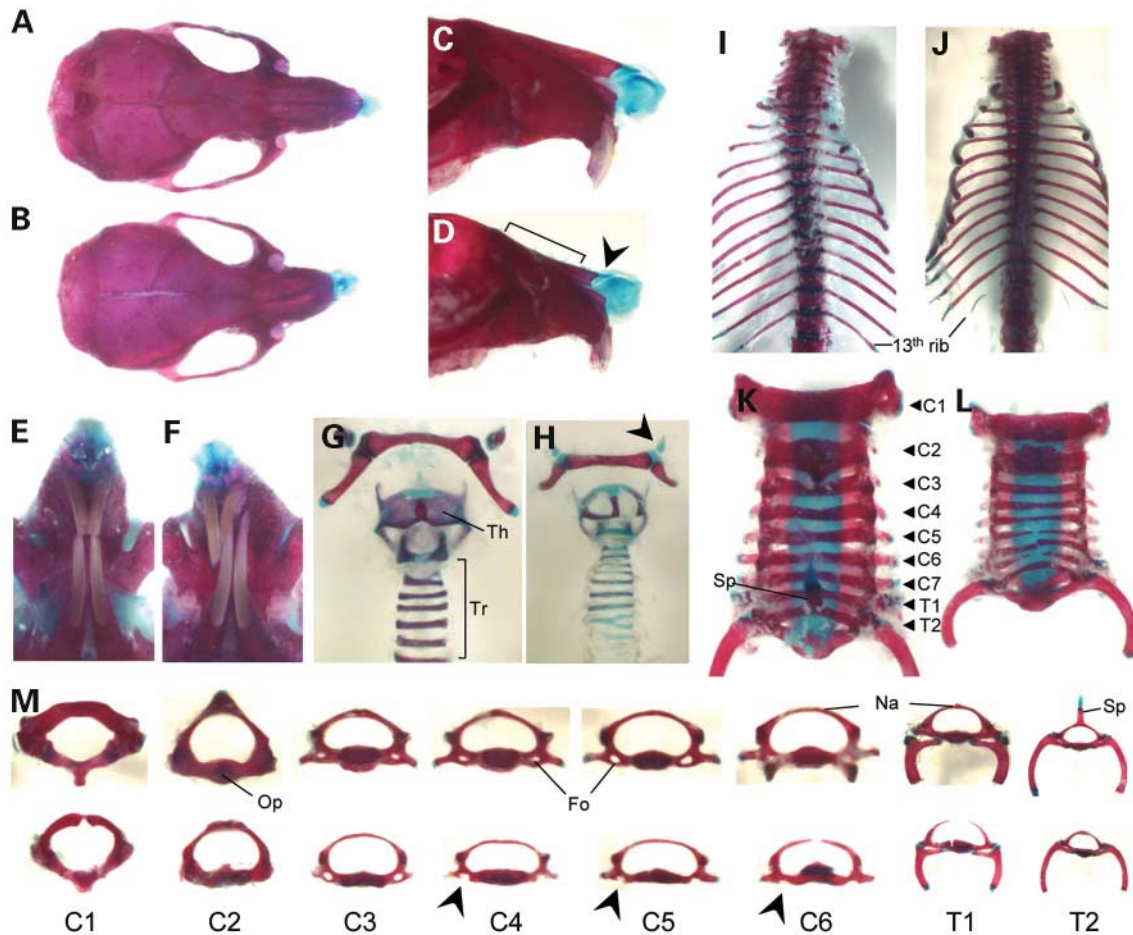


**Figure 6.** Skeleton malformations in one *Rail*<sup>-/-</sup> mouse at 1.5 month (A, B, E, F) and one at 1 month (C, D, G–M) of age. (A–D) Top views and side view of the wild-type (A and C) and *Rail*<sup>-/-</sup> (B and D) skulls. Note the shorter (arrowhead) and concave (bracket) nasal bones in the mutants. (E and F) Incisors of the wild-type (E) and the *Rail*<sup>-/-</sup> (F) mutants. Note the mismatch and outgrowth of upper and lower *Rail*<sup>-/-</sup> incisors. (G and H) Dissected hyoid bone and laryngeal cartilage from wild-type (G) and *Rail*<sup>-/-</sup> mice (H). Note the malformation of thyroid bones and delayed ossification in the small horns of the hyoid bones (arrowhead) in the mutants. (I and J) Frontal views of the rib cages of wild-type (I) and *Rail*<sup>-/-</sup> mutant (J). The 13th rib was thinner and not attached with vertebral body in the mutants. (K and L) Dorsal views of the cervical and upper thoracic region of the wild-type (K) and homozygous (L) skeletons. C1–C7, the first to seventh cervical vertebrae, T1 and T2, the first and second thoracic vertebrae. Note the neural arches in the C5 and C7 were not closed, and the spinal process in the T2 was not evident in the mutants. (M) Dissected vertebrae C1–C6 and T1 and T2 of the wild-type (upper) and *Rail*<sup>-/-</sup> (lower) mice. The transverse foramina in the C4, C5 and C6 vertebrae were not closed (arrowhead) in the mutants. Th, thyroid bone; Tr, trachea; Sp, spinal process; Op, odontoid process; Fo, transverse foramina; Na, Dorsal neural arch.

The statistically significant obesity observed in both *Rail*<sup>+/-</sup> mice and SMS patients with *RAIL* point mutations indicate that *RAIL* impacts body weight in humans and mice. Normal dosage of functional *RAIL* is required for proper energy balance. Haploinsufficiency of *RAIL* greatly increases the tendency of obesity. Studies on the etiology of how *RAIL* affects either energy intake or energy expenditure in animal models will likely aid in the development of weight control programs for SMS patients.

The craniofacial phenotype was strongly affected by the genetic background in both mice with deletions and *Rail*<sup>+/-</sup> mice (15), which suggests the existence of genetic modifiers. In the same genetic background, reduced penetrance and severity of the craniofacial anomalies have been observed in SMS mouse models with smaller deletions compared with those with a large deletion (15). We found that the penetrance of the craniofacial phenotype in *Rail* heterozygous mice was

further reduced. To explain these observations, we propose the following two hypotheses. First, *RAIL* is responsible for the majority of the phenotypes, but other genes deleted in the SMS mouse models function synergistically with *Rail* and modify the phenotypes. It has been suggested that the cardiovascular defects in del22q11/DiGeorge syndrome were caused by haploinsufficiency of *TBX1*, a transcription factor in T-box family, and modified by *VEGF*, a signaling growth factor in PDGF family (20,21). An alternative explanation is that the difference in penetrance of the craniofacial phenotype results from different expression levels of *Rail* in mice. In *Drosophila*, gene expression can be influenced by the pairing of alleles on chromosome homologues, a phenomenon termed transvection (22). It is possible that homologous pairing between the two alleles of *Rail* enhances the transcription of *Rail* in the normal allele through transvection in *Rail*<sup>+/-</sup> mice, thus resulting in reduced penetrance.

**Table 3.** Phenotype in offsprings from heterozygous intercrosses

	<i>Rail</i> genotype <sup>a</sup>			<i>P</i> -value (+/+ versus -/-)
	+/+	+/-	-/-	
Weight of newborn mice (g)	( <i>n</i> = 23) 1.4 ± 0.2	( <i>n</i> = 37) 1.3 ± 0.2	( <i>n</i> = 7) 1.1 ± 0.2	5.6 × 10 <sup>-3</sup>
Skeletal abnormalities: <sup>b</sup>	( <i>n</i> = 7)	( <i>n</i> = 7)	( <i>n</i> = 7)	
Short nasal bone	0	0	7	
Extra cartilaginous element in digit 5 of forelimb	0	0	7	
Curved nasal bone	0	0	4	
Hypoplastic thyroid bone	0	0	7	
Fusion of C1 and C2	0	0	7	
Non-closing of neural arches	0	1	5	
Missing T2 spinal process	0	0	5	
Hypoplasia of the 13th rib	0	0	5	

<sup>a</sup>*Rail*<sup>+/-</sup> mice are from the F2 generation (50% 129 and 50% C57).

<sup>b</sup>Skeletal abnormalities are based on the skeletal preparation on mice at 20 days to 1.5 months of age.

In contrast, for mice with larger or smaller deletions, as one allele of *Rail* and surrounding sequences are deleted, there is no enhancement of transcription for the remaining normal allele. Therefore, the *Rail* expression level in mice with deletion may be lesser than that in *Rail*<sup>+/-</sup> mice, which results in an increased penetrance of the craniofacial phenotype in the mice with deletions. This latter hypothesis is supported by the observations that *Rail* is dosage-sensitive and more severe craniofacial anomalies were present in all mice without functional *Rail*, i.e. *Rail*<sup>-/-</sup> mice. Comparison of the expression levels of *Rail* in mice with larger and smaller deletions as well as *Rail*<sup>+/-</sup> mice examined by quantitative RT-PCR will be performed to further evaluate this hypothesis.

### **Rail is required during different developmental stages**

The majority of *Rail* homozygous mice died *in utero* during gastrulation and organogenesis, indicating that *Rail* is critical in embryonic development. As the phenotype was analyzed on a mixed background, the broad range of embryonic lethality may reflect the significant influence of genetic background that has been observed in the SMS mouse model. The few surviving mice experienced postnatal growth retardation and most of them died before weaning. Thus, *Rail* is also required after birth. One cause of death after birth may be reduced function of the immune system. We found infection in both the lungs and sinuses in one *Rail*<sup>-/-</sup> mouse that died at 6 days of age (data not shown). *Rail* was expressed very well in the thymus and spleen on the basis of X-gal staining (data not shown). Importantly, some SMS patients show a decreased level of immunoglobulins and recurrent infections (1). It is possible that RAI1 functions in the immune system. The postnatal growth delay in *Rail*<sup>-/-</sup> mice might be due to growth hormone (GH) deficiency. *Rail* was expressed

strongly in the Rathke's pouch, the primordial of pituitary gland where GH is secreted. SMS patients usually have short stature and GH deficiency was reported in SMS patients recently (23). In addition, *Rail* is expressed strongly in the thyroid primordium and thyroid deficiency has been reported in SMS patients (1).

The development of the axial skeleton was affected when there was no functional *Rail*. The function of *RAI1* in skeletal development has been suggested by the minor skeletal phenotype observed in SMS patients such as short and broad hands, syndactyly and scoliosis. In both of the *Rail* heterozygous and homozygous mutant mice, we did not observe either obvious scoliosis or short hands or fingers. However, we did find minor defects in the axial skeleton including the skulls. The absence of closure of the dorsal arch in some cervical vertebrae might be secondary to neural tube closure defects.

### **Rail functions in transcriptional regulation**

The function of RAI1 in transcriptional regulation has been suggested by the observations that RAI1 contains a PHD zinc finger that is conserved in the trithorax gene family (12) and RAI1 shares similarity in several domains with TCF20 (24). Our data showed that *Rail* recombinant protein is able to translocate into the nucleus and that *Rail* recombinant protein has transactivation activity, which further support the contention that RAI1 functions as a transcriptional regulator.

RAI1 does not possess a known DNA binding domain as determined by computer analysis. Its transactivation activity is relatively weak in comparison to other typical transcription factors. On the basis of our findings, we propose that RAI1 regulates transcription through chromatin remodeling by interacting with other proteins in chromatin as well as proteins in the basic transcriptional machinery. The PHD domain has been suggested to be a protein-protein interaction domain, and many PHD-containing proteins regulate transcription through a multicomponent chromatin remodeling complex (25,26). To elucidate how RAI1 regulates transcription of other genes, it will be necessary to identify the potential RAI1 complex by co-immunoprecipitation and/or yeast two hybrid experiments. We hypothesize that RAI1 is involved in signal transduction on the basis of the predominant expression of *Rail* in the epithelial cells, such as the AER, endoderm of pharyngeal arches, and otic vesicles, during early embryonic development. RAI1 is inducible by retinoic acid (16). Thus, RAI1 might cooperate with retinoid receptors for the transduction of retinoid signaling. We further hypothesize that RAI1 is a coactivator recruited by retinoid receptors. Both human and mouse RAI1 contain an LxLL motif that is observed in all the coactivators interacting with retinoid receptors (27). Retinoic acid signaling is required for the zone of polarizing activity formation in the chick and normal forelimb growth in the mouse (28,29), which is likely to be mediated through the expression of *Rail* in the AER.

Our data show that *Rail* is a positive transcriptional regulator that is responsible for the craniofacial abnormalities and obesity in SMS mouse models with deletions. The reduced penetrance of craniofacial phenotype reported in *Rail*<sup>+/-</sup> mice suggests the presence of a modifier within the SMCR

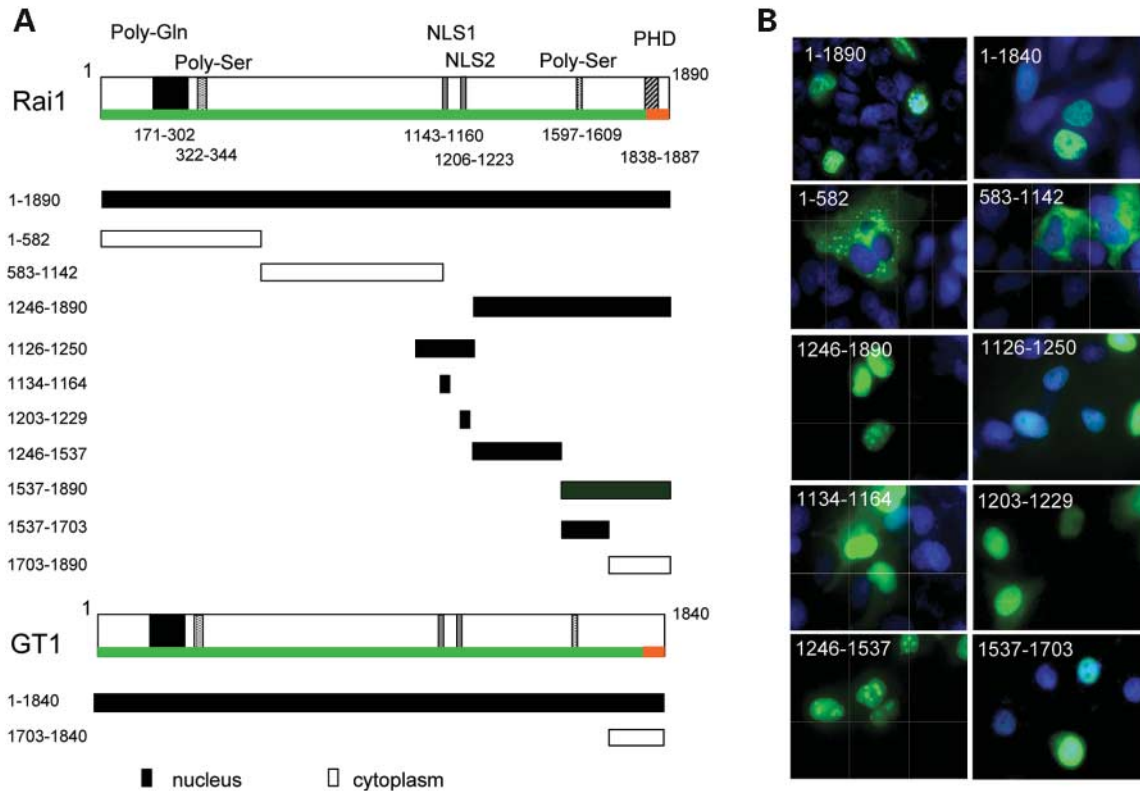


**Figure 7.** Rai1 nuclear localization signals map to four regions. (A) Schematic drawing of the different regions of Rai1 and GT1 fused to the C-terminus of GFP. The top line represents the domain structure of mouse Rai1. The colored horizontal lines underneath indicate the region shared by Rai1 and GT1 (green) and the regions unique to Rai1 or GT1 (orange). Numbers below refer to the amino acid positions. Two nuclear localization signals were predicted previously by computer analysis. (B) Photomicrographs to show the localization of GFP fusion proteins (green). Nuclei were stained by DAPI (blue). The full-length Rai1 or GT1 fused with GFP exclusively localized in the nucleus (upper panel). GFP fusions 1–582 and 583–1142 were exclusively detected in cytoplasm (second panel). Four distinct regions, amino acids 1134–1164, 1203–1229, 1246–1537, and 1537–1703, directed the GFP signal into nucleus (lower three panels).

or reflects reduced expression of *Rai1* due to altered regulation. In addition, the expression pattern of *Rai1* and the embryonic lethality suggest its roles in multiple organs and tissues during mouse embryonic development. It will be interesting to determine whether the behavioral anomalies observed in the SMS *Df(11)17* mouse model (14) are also present in the *Rai1* mutant mice or whether other genes in the SMS critical region are responsible. Recent studies show that *Dexas1* potentiates photic and suppresses non-photic responses of the circadian clock (30). *Dexas1* maps close to *Rai1* and is deleted in the *Df(11)17* SMS mouse model that displays abnormal circadian rhythms (14). BAC complementation studies and double gene targeting will determine what, if any, role that other genes in the SMCR play in specific endophenotypes of the syndrome.

## MATERIALS AND METHODS

### Gene targeting

We isolated two BACs, RP22-135B4 and RP22-223P15, that contain the *Rai1* genomic region by screening a RPCI-22 (129SvEv background) BAC library using *Rai1* specific overgo oligos. Two homology regions were retrieved by recombineering, an efficient recombination system used for

subcloning DNA from BAC clones by gap repair and also for modifying BACs (31). The 5'-homology region consisted of a 3.4 kb *Rai1* genomic fragment spanning from within intron 1 to codon 537 within exon 2, was retrieved into a plasmid with *MC1tkpA* herpes simplex virus thymidine kinase expression cassette. A 3.2 kb fragment of *Rai1* genomic sequence from codon 1790 within exon 2 to within intron 2 serves as the 3'-homology region. The two retrieved regions of homology were ligated together and an *IRES-lacZ-pA-PGK-neo-bPA* cassette (32) was then inserted in between them.

The targeting vector was linearized using *Not1* and electroporated into mouse strain 129SvEv/Brd embryonic stem cells. G418/FIAU-resistant ES cell clones were isolated and screened for targeting events by Southern analysis. The genomic DNA was digested with *EcoR1* and the blots were hybridized with a 625 bp external probe within intron 3 amplified with primers 5'-CGGATCCAGAGAGCAGAAAG-3' and 5'-ACCACTACCCATGTGCCAAT-3'. The targeted clones were confirmed by probing with a 699 bp PCR fragment residing in intron 1 amplified using primers 5'-CAGGATTACAGGCCAGCTTC-3' and 5'-GAAGCTCTGCCCTTGTGAG-3'. Three of these clones were injected into C57BL/6*Tyr<sup>c-Brd</sup>* blastocysts and then transplanted into pseudo-pregnant females. The resulting chimeric males were mated with C57BL/6 *Tyr<sup>c-Brd</sup>* males for germline transmission, and F1

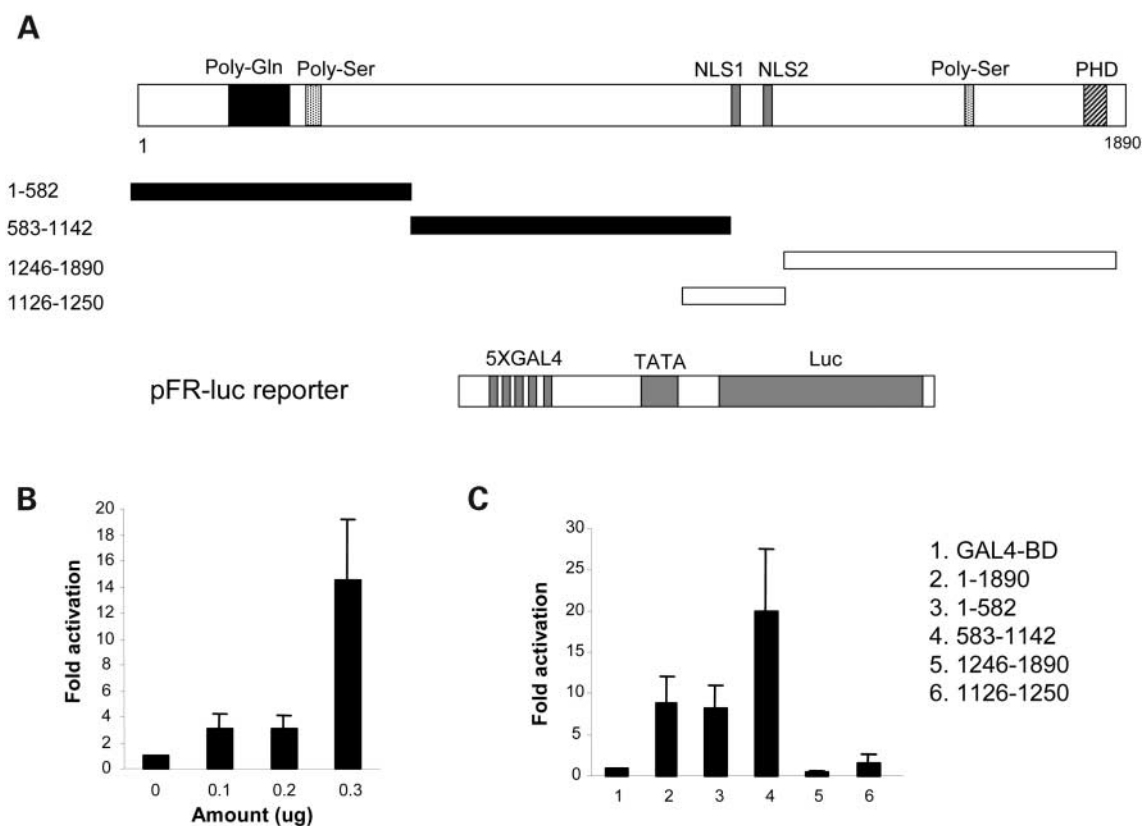


**Figure 8.** Rai1 transactivation domains map to its N-terminus. (A) Schematic drawings of the different regions of Rai1 fused to the C-terminus of GAL4-BD. The fragments with transactivation activity were indicated by black horizontal rectangles and those without activity were indicated by open rectangles. (B) The relative luciferase activity was measured by the co-transfection of different amounts of the expression construct of the full-length Rai1 (1–1890) fused with GAL4-BD and the luciferase reporter plasmid (pFR-luc) into HeLa cells.  $\beta$ -Galactosidase activity was used to normalize variations in transfection efficiency. The highest activity was observed when 0.3  $\mu$ g of GAL4 fusion plasmid was used. (C) Two regions, residues 1–582 (column 3) and residues 583–1142 (column 4), retain transactivation activity.

male progeny was back-crossed with C57BL/6 females to produce N2 mice for weight analysis and craniofacial studies in heterozygous mutants. F1 animals were also intercrossed for homozygous mice. Mice were kept in a mixed background with 50% 129SvEv and 50% C57BL/6. Mice were fed with regular chow with 20% protein and 5.4% fat (PicoLab 5053).

To evaluate the transcript from the targeted allele, total RNA was prepared from the kidneys using Trizol reagent (Gibco). cDNA was made using a 1st strand cDNA synthesis kit for RT-PCR (Roche). The 5'-undeleted region was amplified using primer 1 (5'-ACCTGCGCCAAGTACCAACAC-3') and primer 2 (5'-ACGAGGTTCTTGACCCCTTT-3'); the deleted region was amplified using primer 3 (5'-TCCCCTGAAGTGGGACATAG-3') and primer 4 (5'-GTGTGCAGAGAGGAGGAAAGG-3'); the 3'-undeleted region was amplified using primer 5 (5'-CTTTGAAGTGCCCCAAACAT-3') and primer 6 (5'-AACAGTGGGGTGGGAAGACTG-3').

### Mouse genotyping

Mice were genotyped by PCR on genomic DNA prepared from mouse tails using two pairs of primers. Primers P1F (5'-CCCCTACCACAGCCACTATC-3') and P1R (5'-GAGCCC TGGAGACTTCTG-3') were used to amplify a 427 bp

fragment unique to the wild-type allele and primer P2F (5'-TGGCTACCCGTGATATTGCT-3') was paired with P1R to amplify a 720 bp fragment unique to the targeted allele. DNA prepared from yolk sac was used for genotyping embryos from 8.5 to 18.5 dpc. Yolk sac was incubated in 20–100  $\mu$ l lysis buffer (50 mM KCl, 1.5 mM MgCl<sub>2</sub>, 10 mM Tris-Cl, pH 8.4, 0.5% Tween 20, 1 mg/ml proteinase K) at 55°C for 3 h to overnight. After inactivation of proteinase K at 100°C for 15 min, 2  $\mu$ l was used for a 25  $\mu$ l PCR reaction. The PCR conditions used were 95°C for 15 min for 1 cycle, followed by 42 cycles of 95°C for 30 s, 58°C for 30 s, 72°C for 1 min and then extension at 72°C for 7 min. For embryos at 7.5 dpc, DNA was prepared from the whole embryos lysed in 20  $\mu$ l of lysis buffer and 2  $\mu$ l was used for PCR.

### Whole-mount *in situ* hybridization

Embryos were fixed in phosphate-buffered saline (PBS) containing 4% paraformaldehyde at 4°C overnight. Whole-mount *in situ* hybridization was performed according to standard procedures using digoxigenin-labeled riboprobes (33). The probes used were a 496 bp fragment amplified by primers 5'-CTTTGAAGTGCCCCAAACAT-3' and 5'-AACAGTGGGGTGGGAAGACTG-3', which is unique to

*Rail*, and a 487 bp fragment amplified by primers 5'-ACCTCGCCAAGTACCAACAC-3' and 5'-ACGAGGTTC TTGACCCCTTT-3', which is unique to *GTI*.

### $\beta$ -Galactosidase assay

Embryos were collected in cold PBS and fixed in freshly prepared fixation solution (0.2% glutaraldehyde, 2% formaldehyde, 5 mM EGTA and 2 mM MgCl<sub>2</sub> in 0.1 M phosphate buffer pH7.3). Embryos were then washed three times in rinsing solution (0.01% sodium deoxycholate, 0.02% NP40, and 2 mM MgCl<sub>2</sub> in 0.1 M phosphate buffer pH7.3) for 30 min each, followed by overnight incubation in staining solution (1 mg/ml X-gal, 5 mM potassium ferricyanide and 5 mM potassium ferrocyanide in rinse solution). After staining, the embryos were rinsed briefly in rinse solution, re-fixed in 4% formaldehyde, and dehydrated into 70% ethanol. For histology, embryos were embedded in paraffin, sectioned and counter-stained using eosin.

### Skeletal analysis

Mice were skinned and eviscerated. The carcass was dehydrated in 95% ethanol for 3 days. Staining of cartilage was performed in acid-alcohol solution with 0.05% Alcian blue 8GX (Sigma) 95% ethanol and 20% acetic acid for 2 days. Samples were re-fixed in 95% ethanol for 2 days, followed by clearing in 2% KOH for 2–3 days. Staining of bones was performed in 0.015% of Alizarin red in 1% KOH for 2 days. The stained skeleton was further cleared using 1% KOH and 20% glycerol and stored in 100% glycerol.

### Plasmid constructs

To obtain the full-length *GTI*, an ~5.5 kb fragment covering the complete *GTI* coding region was retrieved into pBlue-script KS from BAC RP22-223P15 through recombineering. To obtain the full-length of *Rail*, a 560 bp fragment covering the 3' end of the *Rail* cDNA was amplified from IMAGE clone 6506272 and replaced with the 3' end of *GTI* downstream from the unique *Xho*I site. To study the subcellular localization, the full-length *Rail* and *GTI* and the different subregions were cloned in frame into the vector pEGFP-C (Clontech). All the subregion fragments in the constructs were generated by PCR using *Pfx* DNA polymerase (Invitrogen) with the exception of region (1–582) was a 1748 bp *Bgl*II/*Eco*R1 fragment digested from the full-length *Rail* plasmid. The integrity of DNA fragments generated by PCR was confirmed by DNA sequencing. To study the transactivation activity, the full-length *Rail* and *GTI* and the different subregions were cloned in frame into the vector pCMV-BD (Stratagene). Fragments were digested from pEGFP fusions and subcloned into pCMV-BD for luciferase reporter assay.

### Subcellular localization studies

HeLa cells were seeded at a density of  $\sim 0.5 \times 10^4$  cells per chamber in a Lab-Tek 4-chamber slide (Nunc) and transfected 24 h later with 0.1  $\mu$ g of the different GFP fusion constructs using lipofectamine 2000 according to the manufacturer's

instructions (Invitrogen). Two days after transfection, cells were washed three times with ice-cold PBS and fixed in 4% paraformaldehyde for 10 min at 4°C. DNA was stained with SlowFade light antifade kit with DAPI (Molecular Probe) for 5 min at room temperature. The subcellular localization of the GFP fusion proteins was determined using a Zeiss Axioplan2 fluorescence microscope.

### Reporter gene assays

Transient transfection of HeLa cells was performed in a 24 well plate using lipofectamine 2000 (Invitrogen). Expression vectors (0.3  $\mu$ g) for GAL4-BD fusions were co-transfected with the luciferase reporter plasmid pFR-Luc (Stratagene) (0.2  $\mu$ g). Plasmid pSV2 $\beta$ gal (0.1  $\mu$ g) was also co-transfected for normalizing variations in transfection efficiency. Cell lysates were prepared 48 h following transfection. Luciferase assays were measured with a luminometer using D-luciferin as substrate in the reaction buffer (100 mM potassium phosphate, pH 7.8, 5 mM ATP, 15 mM MgSO<sub>4</sub>, 1 mM dithiothreitol).  $\beta$ -Galactosidase activities were measured with a chemiluminescent assay kit (Tropix, Bedford, MA, USA). Transfections were performed in triplicate and each cell assay was repeated three times.

### Statistical analysis

Values shown represent the mean  $\pm$  SEM. For differences between two groups, a two-tailed Student's *t*-test was performed using Microsoft Excel (Microsoft office 2001, Redford, Wash). Values of *P* < 0.05 were considered significant.

### ACKNOWLEDGEMENTS

We thank R. Behringer, K. Inoue, B. Morrow and L. Potocki for critical reviews. This work was supported in part by grants from the National Institute for Dental and Craniofacial Research (RO1 DE015210) and the Baylor College of Medicine Mental Retardation Research Center (HD 2406407).

### REFERENCES

- Greenberg, F., Lewis, R.A., Potocki, L., Glaze, D., Parke, J., Killian, J., Murphy, M.A., Williamson, D., Brown, F., Dutton, R. *et al.* (1996) Multidisciplinary clinical study of Smith–Magenis syndrome (deletion 17p11.2). *Am. J. Med. Genet.*, **62**, 247–254.
- Chen, K.-S., Potocki, L. and Lupski, J.R. (1996) The Smith–Magenis syndrome [del(17)p11.2]: clinical review and molecular advances. *MRDD Res. Rev.*, **2**, 122–129.
- Chen, K.-S., Manian, P., Koeuth, T., Potocki, L., Zhao, Q., Chinault, A.C., Lee, C.C. and Lupski, J.R. (1997) Homologous recombination of a flanking repeat gene cluster is a mechanism for a common contiguous gene deletion syndrome. *Nat. Genet.*, **17**, 154–163.
- Greenberg, F., Guzzetta, V., Montes de Oca-Luna, R., Magenis, R.E., Smith, A.C.M., Richter, S.F., Kondo, I., Dobyns, W.B., Patel, P.I. and Lupski, J.R. (1991) Molecular analysis of the Smith–Magenis syndrome: a possible contiguous-gene syndrome associated with del(17)(p11.2). *Am. J. Hum. Genet.*, **49**, 1207–1218.
- Juyal, R.C., Figueroa, L.E., Hauge, X., Elsea, S.H., Lupski, J.R., Greenberg, F., Baldini, A. and Patel, P.I. (1996) Molecular analyses of 17p11.2 deletions in 62 Smith–Magenis syndrome patients. *Am. J. Hum. Genet.*, **58**, 998–1007.

6. Bi, W., Park, S.-S., Shaw, C.J., Withers, M.A., Patel, P.I. and Lupski, J.R. (2003) Reciprocal crossovers and a positional preference for strand exchange in recombination events resulting in deletion or duplication of chromosome 17p11.2. *Am. J. Hum. Genet.*, **73**, 1302–1315.
7. Shaw, C.J., Bi, W. and Lupski, J.R. (2002) Genetic proof of unequal meiotic crossovers in reciprocal deletion and duplication of 17p11.2. *Am. J. Hum. Genet.*, **71**, 1072–1081.
8. Potocki, L., Chen, K.-S., Park, S.-S., Osterholm, D.E., Withers, M.A., Kimonis, V., Summers, A.M., Meschino, W.S., Anyane-Yeboah, K., Kashork, C.D. *et al.* (2000) Molecular mechanism for duplication 17p11.2—the homologous recombination reciprocal of the Smith–Magenis microdeletion. *Nat. Genet.*, **24**, 84–87.
9. Bi, W., Yan, J., Stankiewicz, P., Park, S.-S., Walz, K., Boerkoel, C.F., Potocki, L., Shaffer, L.G., Devriendt, K., Nowaczyk, M.J.M. *et al.* (2002) Genes in a refined Smith–Magenis syndrome critical deletion interval on chromosome 17p11.2 and the syntenic region of the mouse. *Genome Res.*, **12**, 713–728.
10. Vlangos, C.N., Yim, D.K.C. and Elsea, S.H. (2003) Refinement of the Smith–Magenis syndrome critical region to ~950 kb and assessment of 17p11.2 deletions. Are all deletions created equally? *Mol. Genet. Metab.*, **79**, 134–141.
11. Slager, R.E., Newton, T.L., Vlangos, C.N., Finucane, B. and Elsea, S.H. (2003) Mutations in *RAI1* associated with Smith–Magenis syndrome. *Nat. Genet.*, **33**, 466–468.
12. Bi, W., Saifi, G.M., Shaw, C.J., Walz, K., Fonseca, P., Wilson, M., Potocki, L. and Lupski, J.R. (2004) Mutations of *RAI1*, a PHD-containing protein, in nondeletion patients with Smith–Magenis syndrome. *Hum. Genet.*, **115**, 515–524.
13. Walz, K., Caratini-Rivera, S., Bi, W., Fonseca, P., Mansouri, D.L., Lynch, J., Vogel, H., Noebels, J.L., Bradley, A. and Lupski, J.R. (2003) Modeling del(17)(p11.2p11.2) and dup(17)(p11.2p11.2) contiguous gene syndromes by chromosome engineering in mice: phenotypic consequences of gene dosage imbalance. *Mol. Cell. Biol.*, **23**, 3646–3655.
14. Walz, K., Spencer, C., Kaasik, K., Lee, C.C., Lupski, J.R. and Paylor, R. (2004) Behavioral characterization of mouse models for Smith–Magenis syndrome and dup(17)(p11.2p11.2). *Hum. Mol. Genet.*, **13**, 367–378.
15. Yan, J., Keener, V.W., Bi, W., Walz, K., Bradley, A., Justice, M.J. and Lupski, J.R. (2004) Reduced penetrance of craniofacial anomalies as a function of deletion size and genetic background in a chromosome engineered partial mouse model for Smith–Magenis syndrome. *Hum. Mol. Genet.*, **13**, 2613–2624.
16. Imai, Y., Suzuki, Y., Matsui, T., Tohyama, M., Wanaka, A. and Takagi, T. (1995) Cloning of a retinoic acid-induced gene, *GTI*, in the embryonal carcinoma cell line P19: neuron-specific expression in the mouse brain. *Mol. Brain Res.*, **31**, 1–9.
17. Hayes, S., Turecki, G., Brisebois, K., Lopes-Cendes, I., Gaspar, C., Riess, O., Ranum, L.P.W., Pulst, S.-M. and Rouleau, G.A. (2000) CAG repeat length in *RAI1* is associated with age at onset variability in spinocerebellar ataxia type 2 (SCA2). *Hum. Mol. Genet.*, **9**, 1753–1758.
18. Joobar, R., Benkelfat, C., Toulouse, A., Lafrenière, R.G.A., Lal, S., Ajroud, S., Turecki, G., Bloom, D., Labelle, A., Lalonde, P. *et al.* (1999) Analysis of 14 CAG repeat-containing genes in schizophrenia. *Am. J. Med. Genet.*, **88**, 694–699.
19. Allanson, J.E., Greenberg, F. and Smith, A.C.M. (1999) The face of Smith–Magenis syndrome: a subjective and objective study. *J. Med. Genet.*, **36**, 394–397.
20. Vitelli, F. and Baldini, A. (2003) Generating and modifying DiGeorge syndrome-like phenotypes in model organisms: is there a common genetic pathway? *Trends Genet.*, **19**, 588–593.
21. Stalmans, I., Lambrechts, D., De Smet, F., Jansen, S., Wang, J., Maity, S., Kneer, P., von der Ohe, M., Swillen, A., Maes, C. *et al.* (2003) VEGF: a modifier of the del22q11 (DiGeorge) syndrome? *Nat. Med.*, **9**, 173–182.
22. Duncan, I.W. (2002) Transvection effects in *Drosophila*. *Annu. Rev. Genet.*, **36**, 521–556.
23. Spadoni, E., Colapietro, P., Bozzola, M., Marseglia, G.L., Repossi, L., Danesino, C., Larizza, L. and Maraschio, P. (2004) Smith–Magenis syndrome and growth hormone deficiency. *Eur. J. Pediatr.*, **163**, 353–358.
24. Rekdal, C., Sjøttem, E. and Johansen, T. (2000) The nuclear factor SPBP contains different functional domains and stimulates the activity of various transcriptional activators. *J. Biol. Chem.*, **275**, 40288–40300.
25. Aasland, R., Gibson, T.J. and Stewart, A.F. (1995) The PHD finger: implications for chromatin-mediated transcriptional regulation. *Trends Biochem. Sci.*, **20**, 56–59.
26. Kitagawa, H., Fujiki, R., Yoshimura, K., Mezaki, Y., Uematsu, Y., Matsui, D., Ogawa, S., Unno, K., Okubo, M., Tokita, A. *et al.* (2003) The chromatin-remodeling complex WINAC targets a nuclear receptor to promoters and is impaired in Williams syndrome. *Cell*, **113**, 905–917.
27. Bastien, J. and Rochette-Egly, C. (2004) Nuclear retinoid receptors and the transcription of retinoid-target genes. *Gene*, **328**, 1–16.
28. Helms, J.A., Kim, C.H., Eichele, G. and Thaller, C. (1996) Retinoic acid signaling is required during early chick limb development. *Development*, **122**, 1385–1394.
29. Niederreither, K., Vermot, J., Schuhbauer, B., Chambon, P. and Dolle, P. (2002) Embryonic retinoic acid synthesis is required for forelimb growth and anteroposterior patterning in the mouse. *Development*, **129**, 3563–3574.
30. Cheng, H.Y., Obrietan, K., Cain, S.W., Lee, B.Y., Agostino, P.V., Joza, N.A., Harrington, M.E., Ralph, M.R. and Penninger, J.M. (2004) *Dexras1* potentiates photic and suppresses nonphotic responses of the circadian clock. *Neuron*, **43**, 715–728.
31. Copeland, N.G., Jenkins, N.A. and Court, D.L. (2001) Recombineering: a powerful new tool for mouse functional genomics. *Nat. Rev. Genet.*, **2**, 769–779.
32. Bi, W., Deng, J.M., Zhang, Z., Behringer, R.R. and de Crombrughe, B. (1999) *Sox9* is required for cartilage formation. *Nat. Genet.*, **22**, 85–89.
33. Zhao, Q., Behringer, R.R. and de Crombrughe, B. (1996) Prenatal folic acid treatment suppresses acrania and meroanencephaly in mice mutant for the *Cart1* homeobox gene. *Nat. Genet.*, **13**, 275–283.